An Evaluation of the Predictability of Austral Summer Season Precipitation over South America

VASUBANDHU MISRA

Institute of Global Environment and Society, Inc., Center for Ocean–Land–Atmosphere Studies, Calverton, Maryland

(Manuscript received 6 March 2003, in final form 10 July 2003)

ABSTRACT

In this study predictability of austral summer seasonal precipitation over South America is investigated using a 12-yr set of a 3.5-month range (seasonal) and a 17-yr range (continuous multiannual) five-member ensemble integrations of the Center for Ocean–Land–Atmosphere Studies (COLA) atmospheric general circulation model (AGCM). These integrations were performed with prescribed observed sea surface temperature (SST); therefore, skill attained represents an estimate of the upper bound of the skill achievable by COLA AGCM with predicted SST. The seasonal runs outperform the multiannual model integrations both in deterministic and probabilistic skill. The simulation of the January–February–March (JFM) seasonal climatology of precipitation is vastly superior in the seasonal runs except over the Nordeste region where the multiannual runs show a marginal improvement. The teleconnection of the ensemble mean JFM precipitation over tropical South America with global contemporaneous observed sea surface temperature in the seasonal runs conforms more closely to observations than in the multiannual runs. Both the sets of runs clearly beat persistence in predicting the interannual precipitation anomalies over the Amazon River basin, Nordeste, South Atlantic convergence zone, and subtropical South America. However, both types of runs display poorer simulations over subtropical regions than the tropical areas of South America. The examination of probabilistic skill of precipitation supports the conclusions from deterministic skill analysis that the seasonal runs yield superior simulations than the multiannual-type runs.

1. Introduction

The scientific basis for conducting extended range predictions with atmospheric general circulation models (AGCMs) stems from the evidence that the predictable atmosphere's lower boundary, especially sea surface temperature (SST), influences the atmospheric circulations and rainfall in a significant manner at seasonal scales and beyond (Shukla 1998; Shukla et al. 2000).

Continental South America offers a unique region on the earth's surface to diagnose atmospheric climate predictability. It has steep mountains on the western edge of the continent and stradles two active tropical ocean basins, with one of them having the most dominant climate variability, namely, the El Niño–Southern Oscillation (ENSO) phenomenon. These features affect the South American monsoon system on intraseasonal (Misra et al. 2002; Liebmann et al. 1999; Paegle and Mo 1997), interannual (Misra et al. 2002; Paegle and Mo 2002; Diaz et al. 1998; Fu et al. 1999), and decadal (Paegle and Mo 2002; Wainer and Venegas 2002; Venegas et al. 1997; Robertson and Mechoso 1998) time scales. The influence of ENSO on the variability of precipitation over South America has been widely studied with observations (Ropelewski and Halpert 1987, 1989; Diaz et al. 1998; Marengo 1992). Likewise, the teleconnections of precipitation over South America with tropical Atlantic SST have also been diagnosed from observations (Venegas et al. 1997; Diaz et al. 1998; Uvo et al. 1998; Nobre and Shukla 1996). From their theoretical work Campetella and Vera (2003) find that the leading dynamic characteristics of the low-level circulation over South America can be reproduced by the interaction of the mean flow and the Andes Mountains alone without any moist physics. In the observational work of Gan and Rao (1994) they show that the Andes Mountains produce strong modulation in the evolution and propagation of synoptic-scale waves over southern South America. However, because of the biases of the AGCMs owing to their coarse spatial resolution and inaccurate physics, the AGCMs exhibit a prediction skill different from the observed potential predictability.

In this study we will compare and contrast two contemporary ways of running an AGCM with prescribed observed SST to determine the predictability of the austral summer season precipitation over South America. One of the two modes is to integrate the AGCM for a season using observed initial conditions in the same vein as the dynamical seasonal prediction (DSP) following

Corresponding author address: Dr. Vasubandhu Misra, Institute of Global Environment and Society, Inc., Center for Ocean–Land–Atmosphere Studies, 4041 Powder Mill Road, Suite 302, Calverton, MD 20705.
E-mail: misra@cola.iges.org

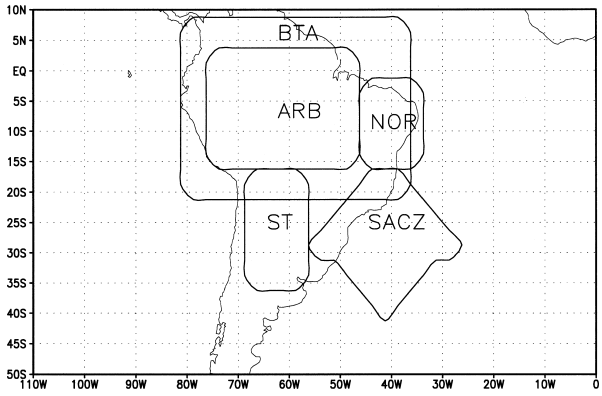

FIG. 1. The outline of the areas referenced in the text.

Shukla et al. (2000). The other approach is to integrate the AGCM for multiple years in the mold of Atmospheric Model Intercomparison Project (AMIP) type runs (Gates et al. 1999). In this study any reference to the skill of the AGCM from either of the two types of AGCM runs points to ''potential skill'' simply because it represents the upper bound of the skill that can be attained by using predicted SST. Ideally, if the model were perfect and run with identical surface boundary conditions then one could easily attribute the differences in the two types of model runs to the sensitivity to initial conditions. However, the AGCMs are far from perfect, especially over South America where the Andes Mountains are poorly resolved. As a result the differences in the two types of model runs cannot be solely due to initial conditions but could also be attributed to the drift or bias in the model.

To compare the two types of model runs in a comprehensive manner we have divided the South American region into four distinct subregions (shown in Fig. 1), namely, the Amazon River basin (ARB), Nordeste (NOR), the South Atlantic convergence zone (SACZ), and subtropical South America (ST). Each of these regions has been identified from observations to have distinct climatology and variability with important contribution to the overall South American monsoon system (Zhou and Lau 1998). Zhou and Lau (1998) note that in the premonsoon phase the center of the upper-level divergence and low-level convergence lies over ARB as a result of strong local convective heating. In the monsoon development phase the convection moves southeastward over southeastern Brazil with the anticyclonic center over the South Atlantic Ocean moving westward and the cross-equatorial flow over the tropical Atlantic intensifying. In the mature stage of the monsoon the SACZ migrates southwestward and the rainfall over the subtropical Andes intensifies substantially. Paegle and Mo (1997) use observed outgoing longwave radiation (OLR) fields to identify a seesaw pattern between the SACZ region and the subtropical plains of South America (ST). They show that the intensification of SACZ is associated with rainfall deficit over ST and vice versa. Misra et al. (2002) showed that a deficit of rainfall over ARB was associated with a stronger low-level jet (LLJ) resulting in higher seasonal precipitation over ST. It is evident from the above discussion that the austral summer season precipitation over South America exhibits high spatial and temporal variability that are part of a larger South American monsoon system. In the following section we briefly describe the model used in this study. In section 3 we explain the design of the experiments followed by section 4 discussing the results. Concluding remarks are provided in section 5.

2. Model description

The AGCM used in this study is version 2.2 of the Center for Ocean–Land–Atmosphere Studies (COLA) global spectral model at T42 (2.5°) horizontal resolution and 18 levels (COLA AGCM). This version of the model uses the dynamical core of the National Center for Atmospheric Research Climate Community Model version 3 (CCM3) described in Kiehl et al. (1998). The dependent variables of the model are spectrally treated except the moisture variable, which is advected using the semi-Lagrangian technique. The parameterization of deep convection follows the relaxed Arakawa–Schubert scheme (Moorthi and Suarez 1992). The parameterization of shallow convection follows Tiedtke (1984). The subgrid-scale exchange of heat, momentum, and moisture is accomplished via a turbulent closure scheme, level 2.0 (Mellor and Yamada 1982). The diagnostic cloud fraction and optical properties are similar to CCM3 (Kiehl et al. 1998) and are described in Dewitt and Schneider (1997). The terrestrial and shortwave radiation follows Harshvardhan et al. (1987) and Davies (1982), respectively. A fourth-order horizontal diffusion is applied to all variables except the moisture variable. A mean surface orography (Fennessy et al. 1994) is used to represent surface elevation. Dry convective adjustment and gravity wave drag are not invoked in the model integrations. The atmospheric model is coupled to the Simplified Simple Biosphere model (SSiB) documented in Xue et al. (1991, 1996).

3. Design of experiments

For both the AMIP- and DSP-type runs the surface boundary condition of SST is obtained from the monthly mean Hadley Centre Sea Ice and Sea Surface Temperature (Hadisst) dataset (Parker et al. 1999). This is available monthly on a $1° \times 1°$ grid from 1870 to the present. The soil moisture fields are obtained from a 2-yr climatology of the Global Soil Wetness Project (Dirmeyer and Zeng 1999).

Five-member ensembles are made for both the AMIP- and DSP-type runs. The DSP runs are made for years from 1984/85 to 1995/96 starting from 0000 UTC 15 December of the corresponding year through 1200 UTC 31 March of the following year. The AMIP runs start

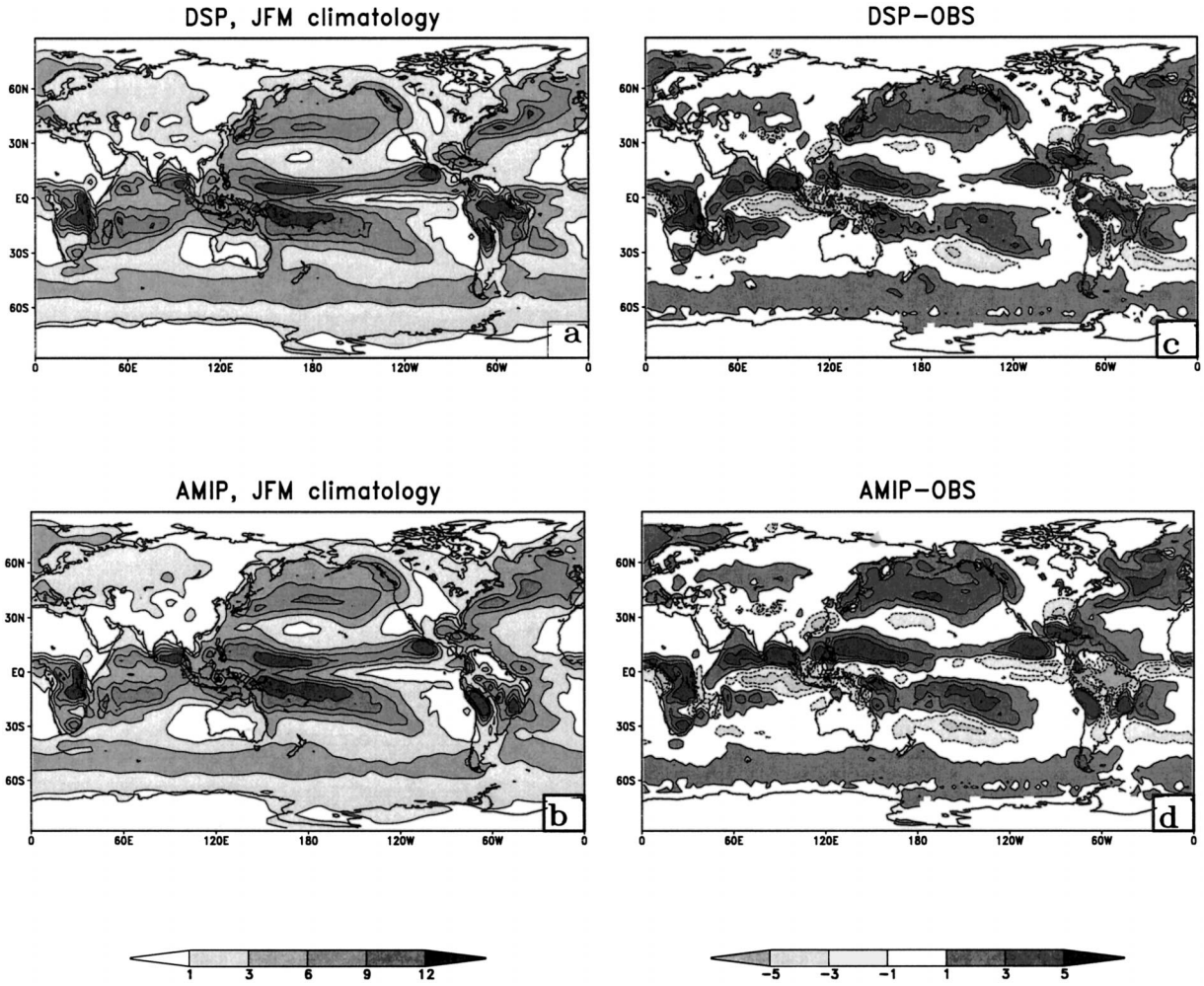

FIG. 2. The mean JFM climatology from (a) DSP- and (b) AMIP-type runs. The systematic errors of JFM precipitation in (c) DSP- and (d) AMIP-type runs. The units are in mm day^{-1}.

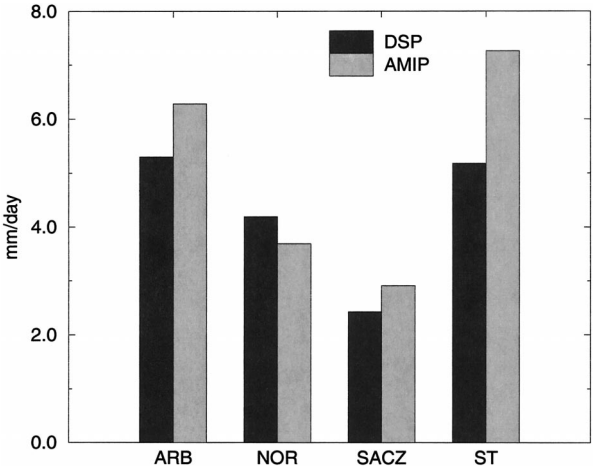

FIG. 3. The rmse of mean JFM precipitation climatology over areas delineated in Fig. 1. The units are in mm day^{-1}.

from 0000 UTC 15 December, 1978 and end on 1200 UTC 31 December, 1996. The atmospheric initial conditions for all these model runs are generated by initially running the COLA AGCM from the National Centers for Environmental Prediction–National Center for Atmospheric Research (NCEP–NCAR) reanalysis for 0000 UTC December 15 of the year for a week and resetting the date on the restart file to the initial date. This procedure is repeated recursively 5 times to generate initial conditions for the other ensemble members (Misra et al. 2003; Kirtman et al. 2001). This perturbation technique therefore distinguishes the ensemble members from synoptically independent atmospheric initial conditions that it generates during the same season.

The model results are verified against the Climate Prediction Center (CPC) Merged Analysis Precipitation (CMAP) dataset (Xie and Arkin 1997) made available on 2.5° × 2.5° latitude–longitude grid. It should be noted that while there is the benefit of the global coverage of

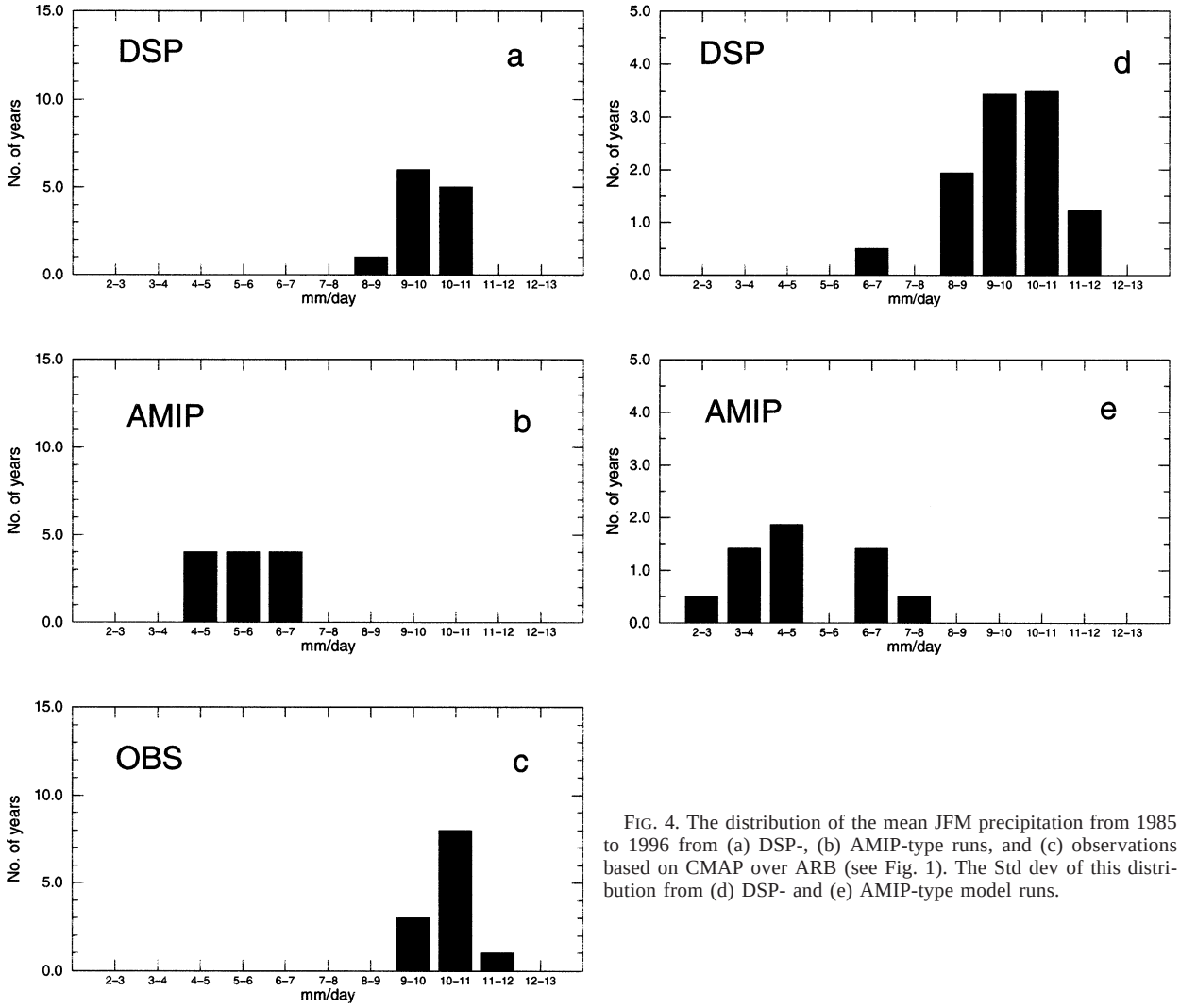

FIG. 4. The distribution of the mean JFM precipitation from 1985 to 1996 from (a) DSP-, (b) AMIP-type runs, and (c) observations based on CMAP over ARB (see Fig. 1). The Std dev of this distribution from (d) DSP- and (e) AMIP-type model runs.

the CMAP dataset, its satellite-based rainfall estimates can sometimes have large observational errors (Krishnamurthy and Shukla 2001). For deterministic skill evaluation the ensemble mean is used. It should be noted here that in the case of DSP-type runs the first 15 days of the integration are neglected to account for spinup issues. Furthermore, to be able to compare and contrast the AMIP- and DSP-type runs, only the results from the AMIP-type runs between 1985 and 1996 are evaluated.

4. Results

We shall first discuss the deterministic skill followed by the probabilistic skill of the model. In this study we shall only focus on the seasonal mean January–February–March (JFM) precipitation.

a. Deterministic skill

In analyzing the deterministic skill the ensemble mean of the corresponding AGCM run is compared with observations. The notion here is that the ensemble mean is the best estimate of the model results and provides equal weighting to each of the ensemble members, thereby implying that the probability of occurrence of any one ensemble model member realization is equal to that of any other member.

In this section we will first assess the model climatology followed by a discussion on interannual variability.

1) MODEL CLIMATOLOGY

The 12-yr (1985–96) model climatology of mean JFM precipitation from DSP- and AMIP-type runs of the COLA AGCM are shown in Figs. 2a,b, respectively. The corresponding errors of the DSP- and AMIP-type model climatology are shown in Figs. 2c,d. Although the large-scale distribution of precipitation in both models is reasonable, the errors in some parts of the globe, especially in the Tropics, are quite large. The split in-

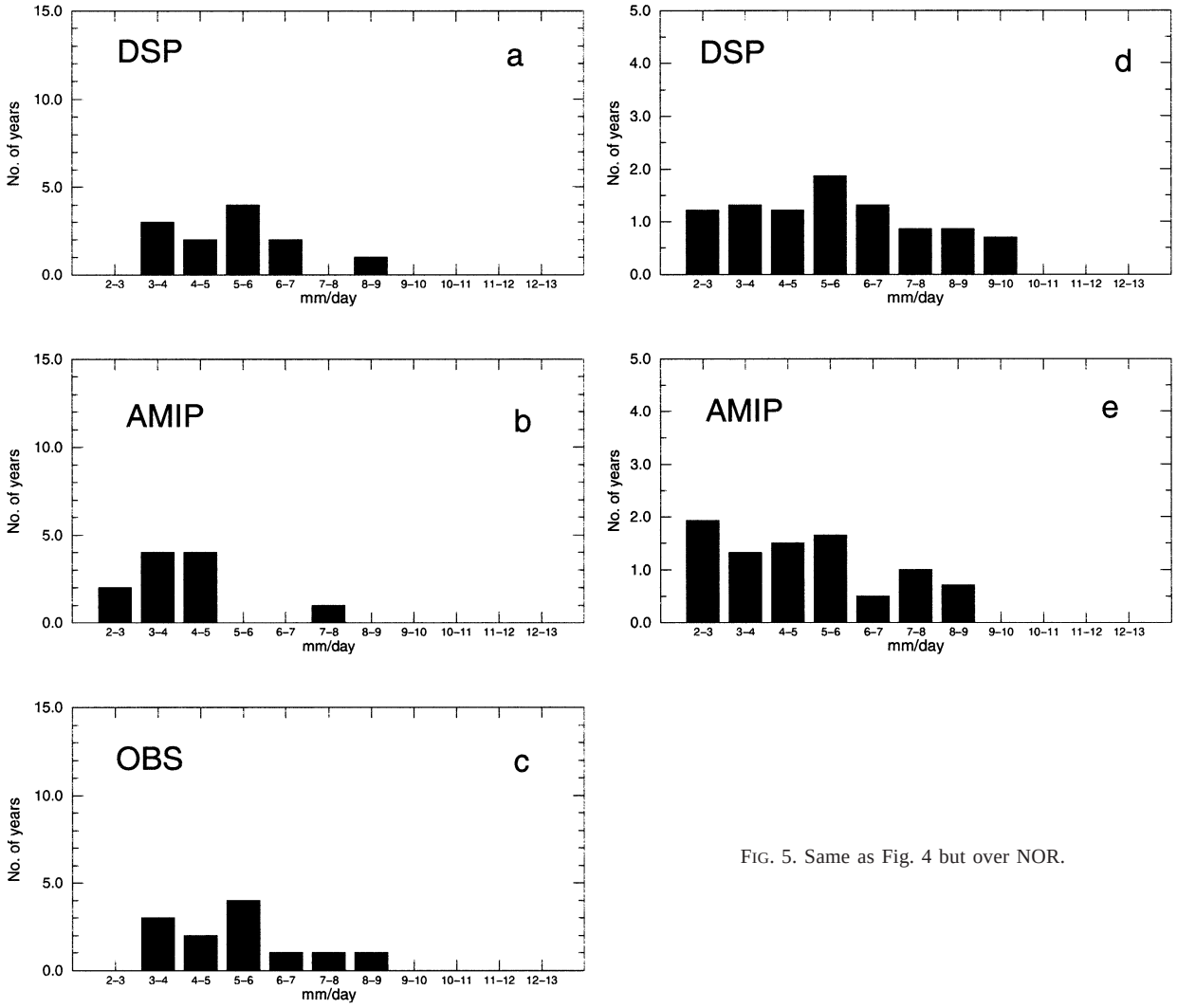

FIG. 5. Same as Fig. 4 but over NOR.

tertropical convergence zone (ITCZ) over the tropical Pacific Ocean is troubling in both the DSP- and AMIP-type runs. Interestingly, the model climatological errors are quite similar in most regions in both AMIP- and DSP-type runs except over South America. In the central Amazon there is a strong dry bias in the AMIP-type runs while the bias is wet in the DSP-type runs. It should also be noted that the banded structure of precipitation over central tropical South America is more prominent in the AMIP- than in the DSP-type runs. Furthermore, the wet bias over the western tropical Atlantic is also substantially reduced in the DSP-type runs relative to AMIP. The root-mean-square error (rmse) over the areas outlined in Fig. 1 are shown in Fig. 3. It is seen in Fig. 3 that the DSP runs have substantially reduced the errors in all the regions except over the Nordeste region where the AMIP runs show a marginal improvement. Nordeste is an area that has shown distinct teleconnections with tropical Pacific and Atlantic SSTs, which have been exploited with some success in predicting the austral summer and fall seasonal precipitation (Folland et al. 2001; Cavalcanti et al. 2002)

In Figs. 4a,b,c we have plotted the distribution of the ensemble mean precipitation rates for JFM between 1985 and 1996 over ARB (see Fig. 1) from the DSP-type, AMIP-type model runs, and observations, respectively. The standard deviation of this distribution across the ensemble mean for DSP- and AMIP-type runs are plotted in Figs. 4d,e, respectively. This standard deviation is obtained by first computing the distribution for each of the ensemble members and then obtaining the standard deviation for each bin of the distribution from the ensemble mean (expressed mathematically in appendix A). The observations indicate that the mean JFM precipitation rates are skewed toward higher precipitation rates with 10–11 mm day^{-1} occurring in 8 of the 12 yr analyzed. However, the distribution of the AMIP-type runs simulate light to medium precipitation rates, which are not verifiable from observations. The DSP-type model integrations simulate higher precipitation

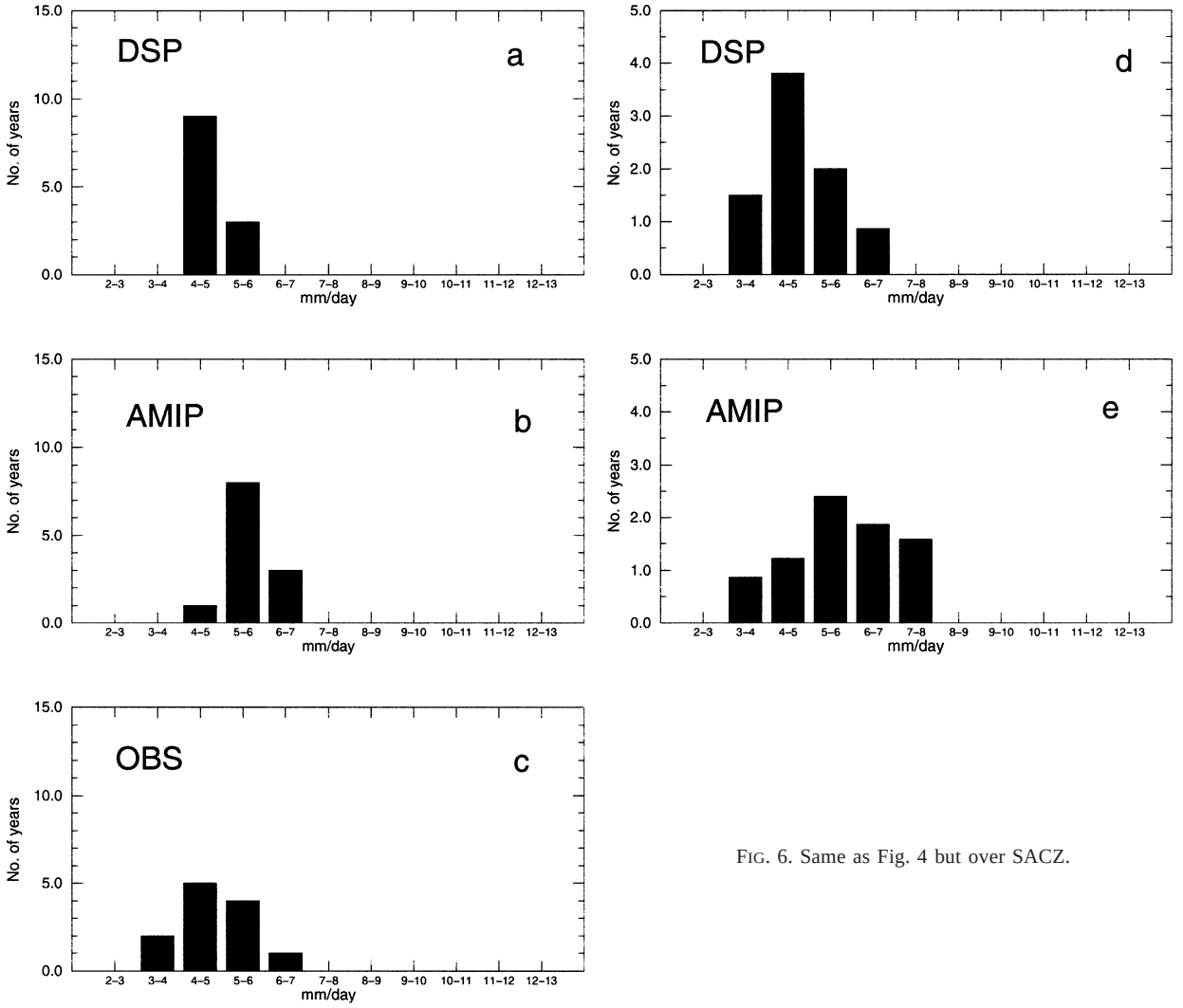

FIG. 6. Same as Fig. 4 but over SACZ.

rates for the season as in observations. The DSP-type runs also show significant intraensemble variability in nearly the same precipitation bins populated by the ensemble mean indicating the sensitivity of the distribution to initial conditions. The AMIP runs also show intraensemble variability in low to medium precipitation rates.

Likewise we have plotted the distribution of the ensemble mean JFM precipitation rates over NOR and its standard deviation in Fig. 5. It is clearly seen from this figure that the DSP-type runs have a more realistic distribution of precipitation rates. The DSP-type runs show that the 5–6 mm day^{-1} category occurs most often, as in observations, followed by 3–4 mm day^{-1}. The AMIP-type runs are skewed more toward the lower precipitation rates with barely any precipitation rate over the 4–5 mm day^{-1} category. The standard deviation across the ensemble shows that the intraensemble variability is more prominent in lighter precipitation rates in AMIP-type runs while it is quite uniformly distributed accross a broad spectrum of precipitation rates in the DSP-type runs.

The distribution of ensemble mean JFM precipitation rates and its standard deviation over SACZ and ST areas are indicated in Figs. 6 and 7, respectively. Over these areas, both model integration types display a distribution different from the observations and show comparatively more intraensemble variability than over the other two tropical areas of ARB and NOR examined earlier.

The discussion thus far indicates that the DSP-type model runs exhibit a better mean JFM precipitation climatology than the AMIP runs for the most part. This suggests that the COLA AGCM has a severe drift over the area that affects the model climatology when long-range simulations are made. However, it is also plausible that the observed climatology over tropical and subtropical South America is significantly governed by the internal variability component that is initial condition

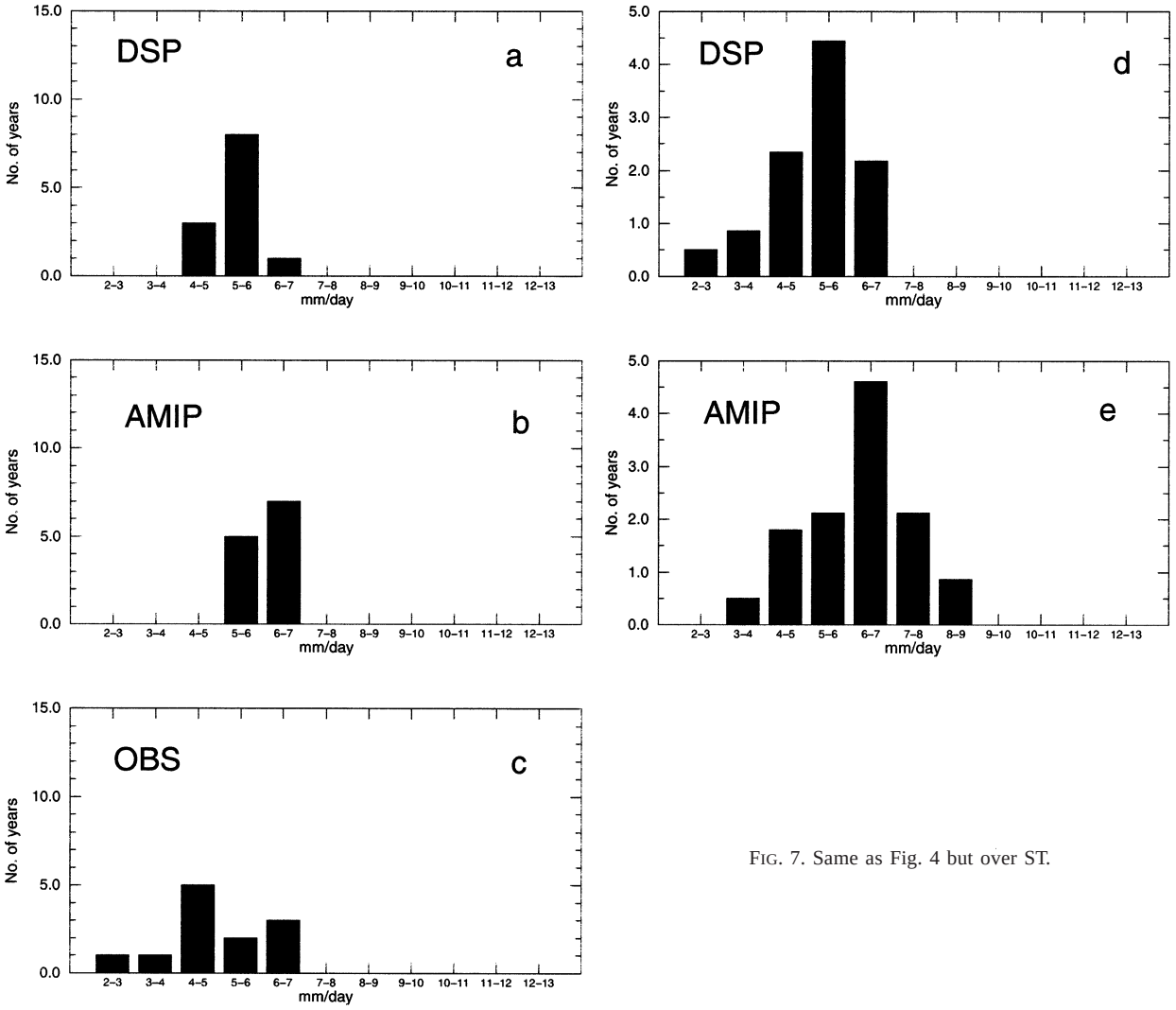

FIG. 7. Same as Fig. 4 but over ST.

dependent. This could also explain to some extent the improved climatology of the DSP-type runs.

2) INTERANNUAL VARIABILITY

In Fig. 8 we show the correlation between global SST and the area-averaged mean JFM precipitation over a big tropical area (BTA in Fig. 1) from (a) DSP-, (b) AMIP-type model runs, and (c) observations. These correlations are computed for the years 1984/85–1995/96. The teleconnection of BTA mean JFM precipitation with the equatorial central and eastern Pacific Ocean in the DSP-type runs conforms with observations. The AMIP-type runs exhibit this teleconnection over the central equatorial Pacific Ocean and over subtropical oceans in both hemispheres. In a related observational study Paegle and Mo (2002) also find that the first rotated empirical orthogonal function (EOF) pattern of precipitation, with large weight over northern tropical, subtropical South America, and over Nordeste, is linked to ENSO in the Pacific Ocean. The COLA AGCM shows significant correlations with tropical South Atlantic SSTA in both model-type runs, which are not seen in the observations (Fig. 8a). However, Paegle and Mo (2002) note that the second rotated EOF of precipitation in their study, with loadings over northeast Brazil and Colombia, show significant correlations with tropical South Atlantic SST anomalies. Furthermore, they also show that the fourth EOF, with loadings over Nordeste and subtropical South America, have linkages with significant correlations with subtropical Pacific Ocean SST anomalies. This is also seen in the DSP- and AMIP-type model runs of the COLA AGCM but with opposite signs. However, the teleconnections of the precipitation with the subtropical Indian and Atlantic Oceans may be unique to the COLA AGCM and is unverifiable from observational studies.

In Fig. 9 we have plotted the normalized standard deviation (NSD) following Misra et al. (2003), which is a measure of the signal-to-noise ratio. The details of

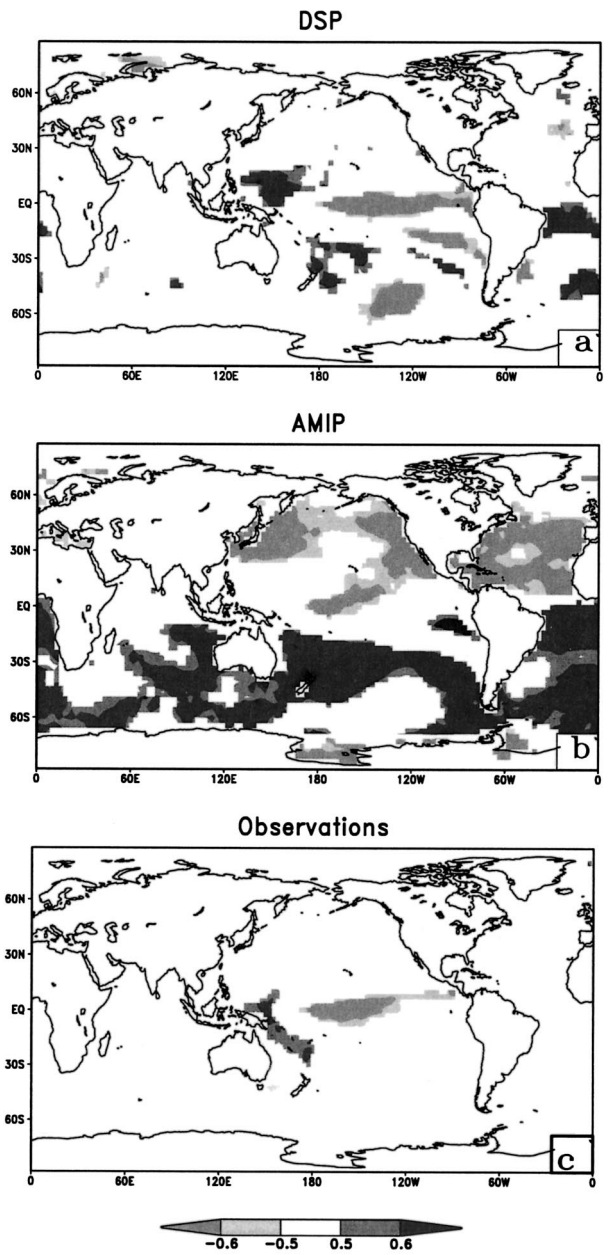

FIG. 8. The correlation of area-averaged JFM precipitation over BTA (see Fig. 1) from (a) DSP-, (b) AMIP-type model runs, and (c) observatons based on CMAP with contemporaneous observed global SST. Only correlations with confidence interval over 90% are plotted.

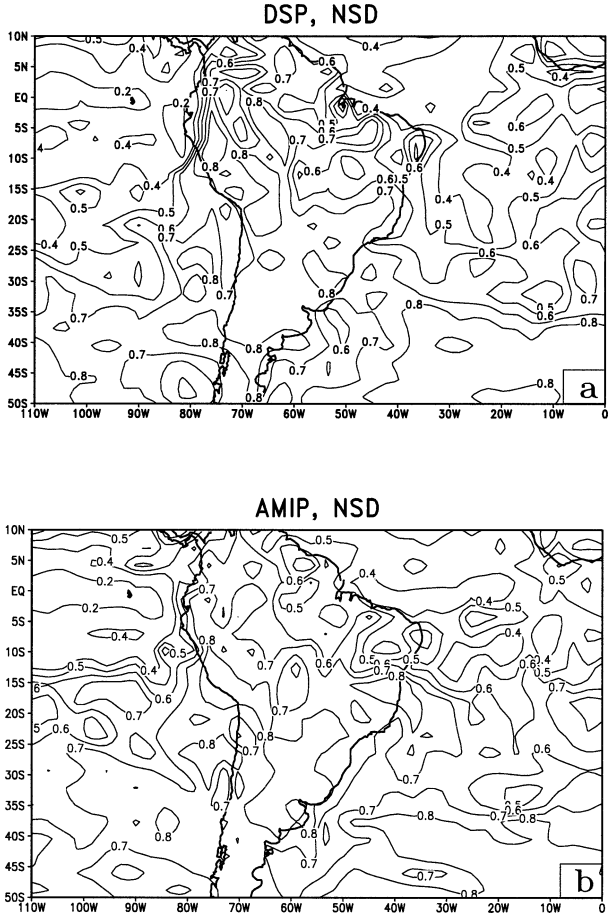

FIG. 9. The NSD (see text) from (a) DSP- and b) AMIP-type model runs.

NSD are provided in appendix B. A NSD of 1(0) would indicate model noise (signal) as the dominating factor. At first glance Fig. 9 shows that NSD in both model-type runs are comparable, with both model run types displaying more noise in the subtropics than in the Tropics and similar NSD over the oceans. However, there are subtle differences, for example, slightly higher (lower) model noise over ST (northeast Brazil, NOR, and northern ARB) in the AMIP-type runs. A relatively smaller ratio of NSD in the AMIP runs especially over land does not necessarily translate to improved skill of the model owing to large systematic errors of the model. For example, the relatively lower NSD found in northeastern ARB in Fig. 9b does not reflect an improved climatology (Fig. 2b) or an improved simulation of the variability as discussed in the following passage. The low NSD ratio over tropical South America is a reflection of its higher signal content from teleconnection patterns with the neighboring ocean basins (Fig. 8).

In Fig. 10 we display the interannual anomalies of the ensemble mean JFM precipitation for the four domains over the ARB, NOR, SACZ, and ST areas from the DSP- and AMIP-type runs and observations. The correlations of the ensemble mean, the individual ensemble members, and the observed persistence of precipitation from the previous season of October–November–December with the observed precipitation for JFM are also indicated in the figure. It is clearly seen that both model-type runs exceed the correlation of the persistence from the previous season in all four domains. The correlations from the DSP-type runs are much high-

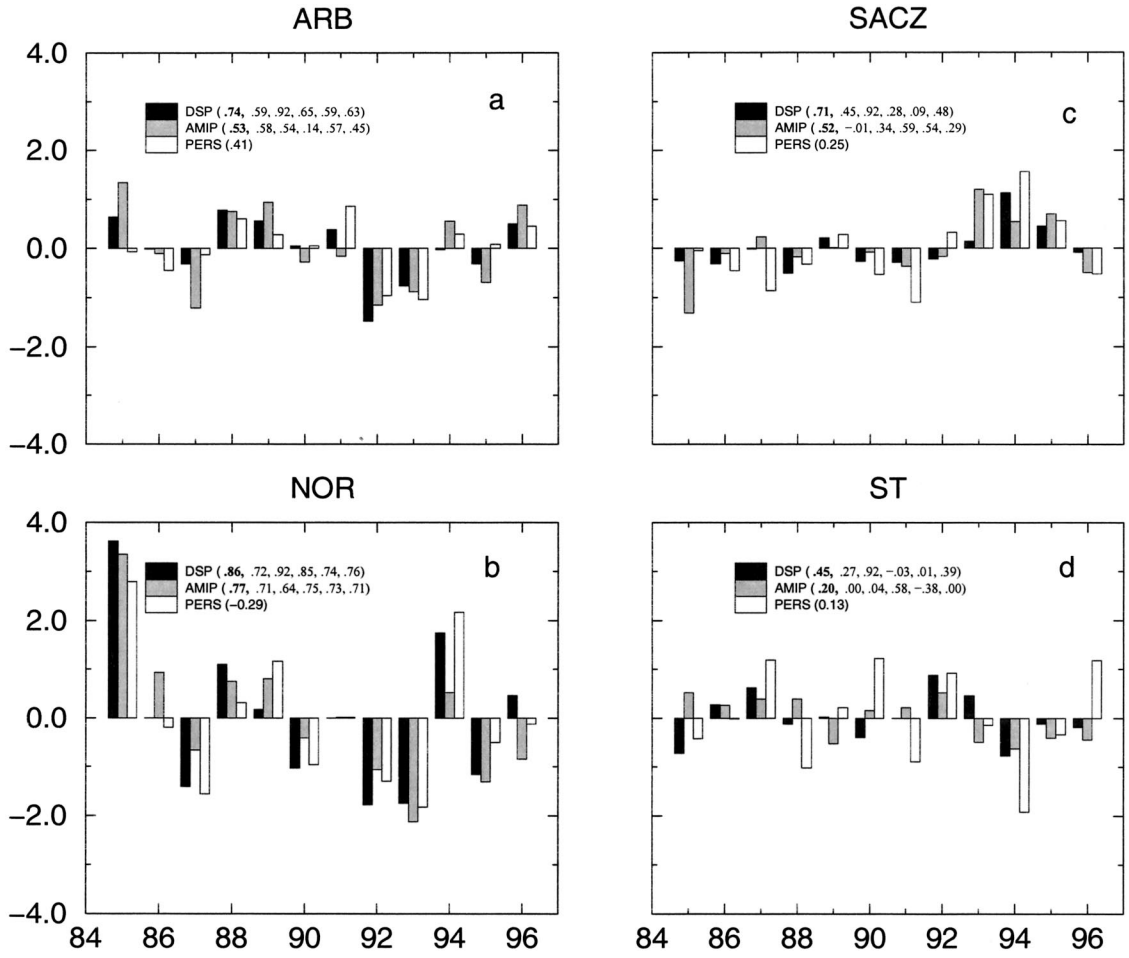

FIG. 10. The interannual anomalies of precipitation from the ensemble mean of DSP- and AMIP-type model runs are compared with observed persistence (PERS) over (a) ARB, (b) NOR, (c) SACZ and (d) ST regions (see Fig. 1). The unit along the ordinate is mm day^{-1}. The anomaly correlations of the precipitation from the ensemble mean (in bold) and the individual ensemble members with observations are indicated in the legend. The correlations indicated with PERS in the legend correspond to that of the observed persistence from the previous season of Oct–Nov–Dec.

er than that from the AMIP runs. Folland et al. (2001) indicate a high degree of predictability over Nordeste from their modeling and observational studies, which they attribute to the influence of the tropical Atlantic and Pacific SST. Also in this study the correlations over Nordeste are appreciably higher compared to other domains. The correlations over Nordeste displayed by the models are relatively quite robust among the ensemble members in both model-type runs. The correlations over the subtropical regions of SACZ and ST show comparatively more spread among the ensemble members and are relatively lower in magnitude (especially over ST) than in the tropical regions of ARB and NOR.

TABLE 1. Definition of probability thresholds used in the ROC analysis for five-member ensembles.

No. of members indicating the event	Probability threshold (%)
Two or more	40
Three or more	60
Four or more	80

b. Probabilistic skill

Recent studies (Kirtman 2002; Palmer et al. 2000) indicate that probabilistic forecast skill assessement provides useful additional information that cannot be gleaned from a deterministic skill evaluation. Brankovic and Palmer (1997) show that extended range atmospheric prediction derives principally from the synergy of the atmosphere with the predictable atmosphere's lower boundary conditions, particularly the SST. They also assert that the SST anomalies impact the phase–space geometry of the whole atmospheric climate attractor rather than a single phase–space trajectory, which can be estimated only from the changes to the atmospheric probability distribution function (PDF)

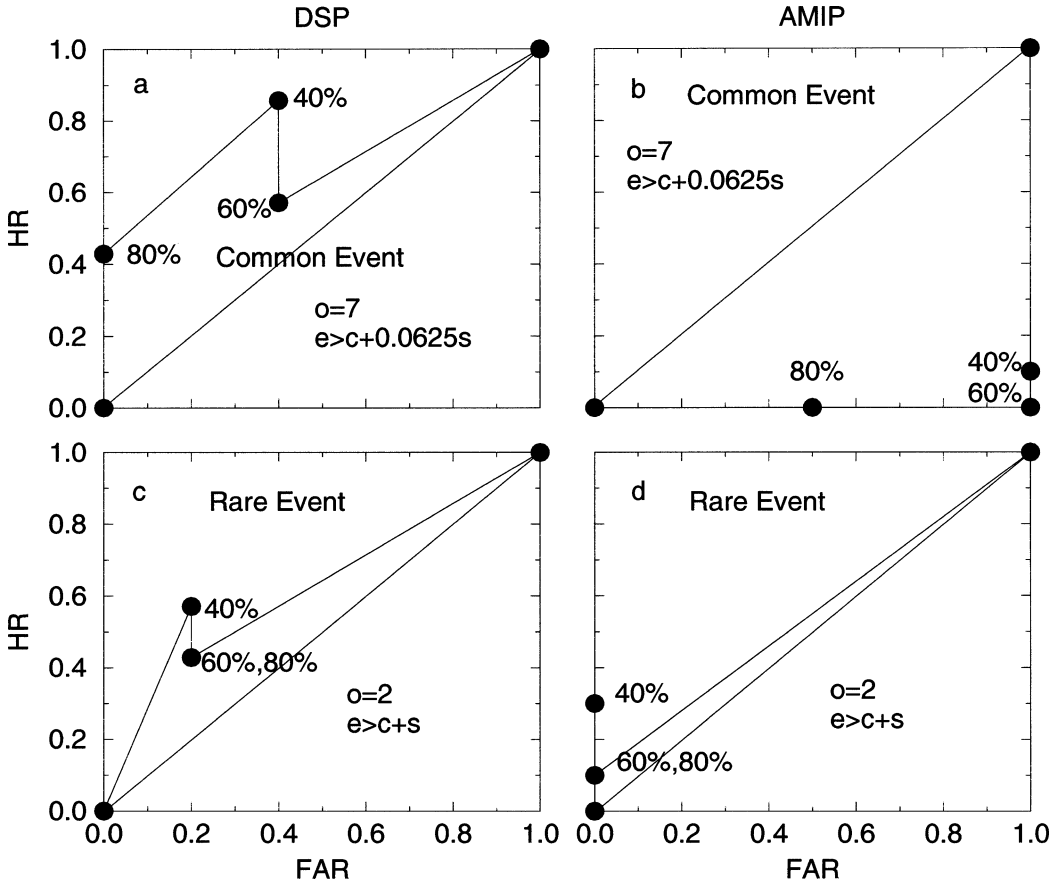

FIG. 11. The ROCs (see text for explanation) over ARB for common occurrence event (*e*) from (a) DSP- and (b) AMIP-type runs. Similarly, ROCs over ARB for rare occurrence event (*e*) from (c) DSP- and (d) AMIP-type runs. The observed occurrences (*o*) from 12 possible cases are indicated in the legend along with the definition of the categorical event. Here, *c* and *s* correspond to the climatology and the associated std dev from observations. FAR and HR refer to false alarm rate and hit rate, respectively (see appendix C for their definition). The probability thresholds are indicated beside the points in the graph.

over atmospheric states. In his study Kirtman (2002) provides compelling evidence that probabilistic skill assessment of climate forecasts including that of SST anomalies are complementary to deterministic skill evaluation.

Here, the probabilistic skill is evaluated using relative operating characteristic (ROC) curves following Graham et al. (2000). The ROCs are obtained by plotting false alarm rates against hit rates (see appendix C) for different probability thresholds. The definition of the probability thresholds for the five-member ensembles in this study are given in Table 1. In Fig. 11, ROC for ARB is plotted for two type of events, namely, common and rare events for both the DSP- and the AMIP-type runs. The common occurence event is defined when an event occurs equal to or greater than 50% of the time in observations. For example, in the case of ARB (Fig. 11a), the common event is defined if the observed mean JFM precipitation for the year exceeds observed mean JFM climatology (*c*) plus 0.0625 times its standard deviation (*s*). The rare event is defined when it occurs equal to or less than 20% of the time in observations. This is defined in the case of the ARB (Fig. 11b) when observed JFM precipitation for the year exceeds the observed mean JFM climatology plus one standard deviation. It was necessary to classify these two types of events because van den Dool and Toth (1991) state that low skill near the mean could sometimes be a feature of the categorical definition rather than having a physical explanation. The DSP run exhibits reasonable skill in the common occurrence event over ARB. However the AMIP runs show no skill at all probability thresholds. In the category of the rare event, the DSP-type runs show better skill than climatology but less than that displayed in the occurrence of the common event. The AMIP-type runs show marginal improvement over climatology at all probability thresholds compared to its results in the common occurrence event.

Similarly, we have plotted the ROC curves for the NOR region in Fig. 12. Here, both AMIP- and DSP-

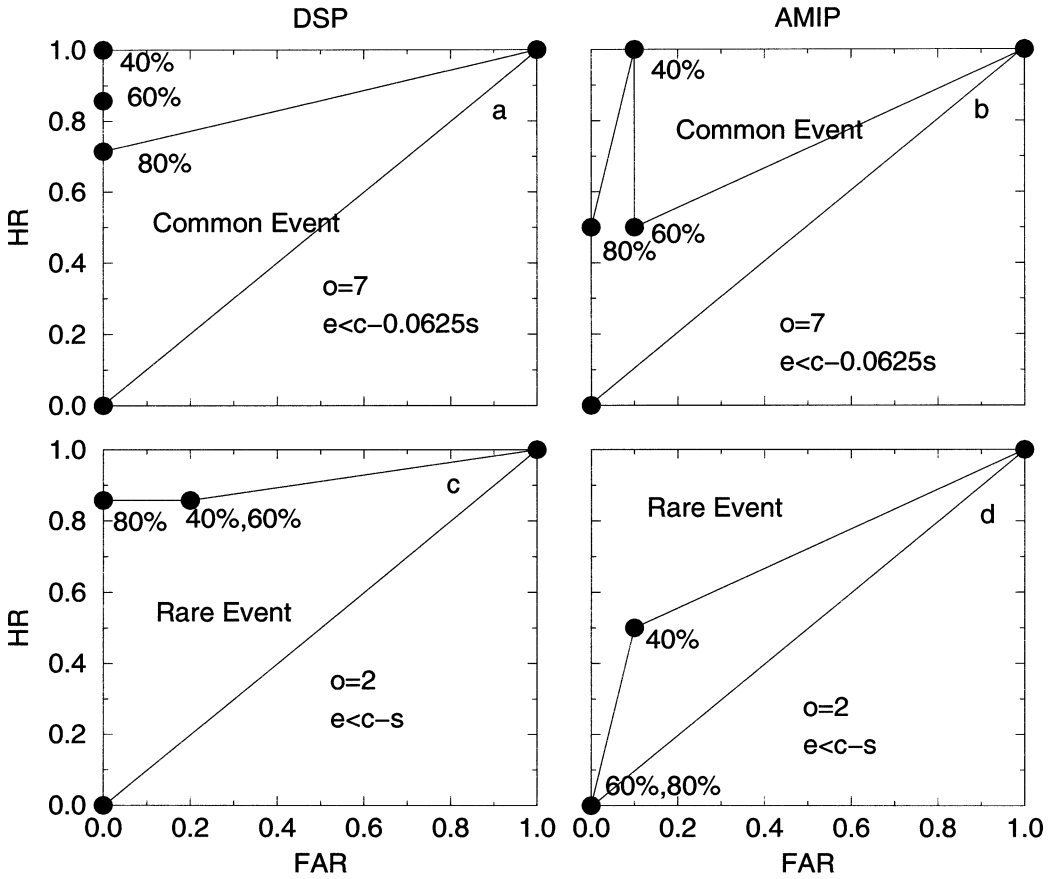

FIG. 12. Same as Fig. 11 but over NOR.

type runs show substantial skill over the climatology. Interestingly, the false alarm rate for the common event category in the DSP runs are zero for all probability thresholds examined in this study. For the rare event category, the probabilistic skill of the DSP-type runs are nearly comparable to that of the common event in Fig. 12a. In the case of AMIP-type runs, there is some skill at the 40% probability threshold but at higher probability thresholds there is none.

The ROC curves over the SACZ region are shown in Fig. 13. The DSP-type runs exhibit substantial probabilitic skill over climatology in both the common and rare events category. As in the case over ARB, the AMIP-type runs show no skill in the common event category over the SACZ region, with marginal improvements seen in the rare event category.

Finally, in Fig. 14 we show similar ROC curves over the ST region. Here, we see that the DSP-type runs show nearly the same skill as in the SACZ region for the common event category. However, in the rare event category this skill displayed by the DSP-type runs are substantially reduced. The AMIP-type runs exhibit comparatively poor skill especially in the rare event category where it is no better than climatology at all probability thresholds.

5. Conclusions

The objective of this study was to evaluate the predictability of austral summer season (JFM) precipitation over South America in the COLA AGCM. This task was accomplished by making a direct comparison of the potential skill in two contemporary modes of running an AGCM; namely, the DSP mode (seasonal integration) and AMIP mode (multiyear integration) under controlled conditions that involved using the same model, same surface boundary conditions, and the same horizontal and vertical resolution.

The following is shown from the examination of the deterministic skill in the COLA AGCM:

- The DSP-type runs uniformly exhibit a better climatology of mean JFM precipitation over the ARB, SACZ, and ST regions relative to AMIP-type runs. However, the AMIP-type runs show marginal improvement in the mean JFM precipitation climatology over the NOR region.

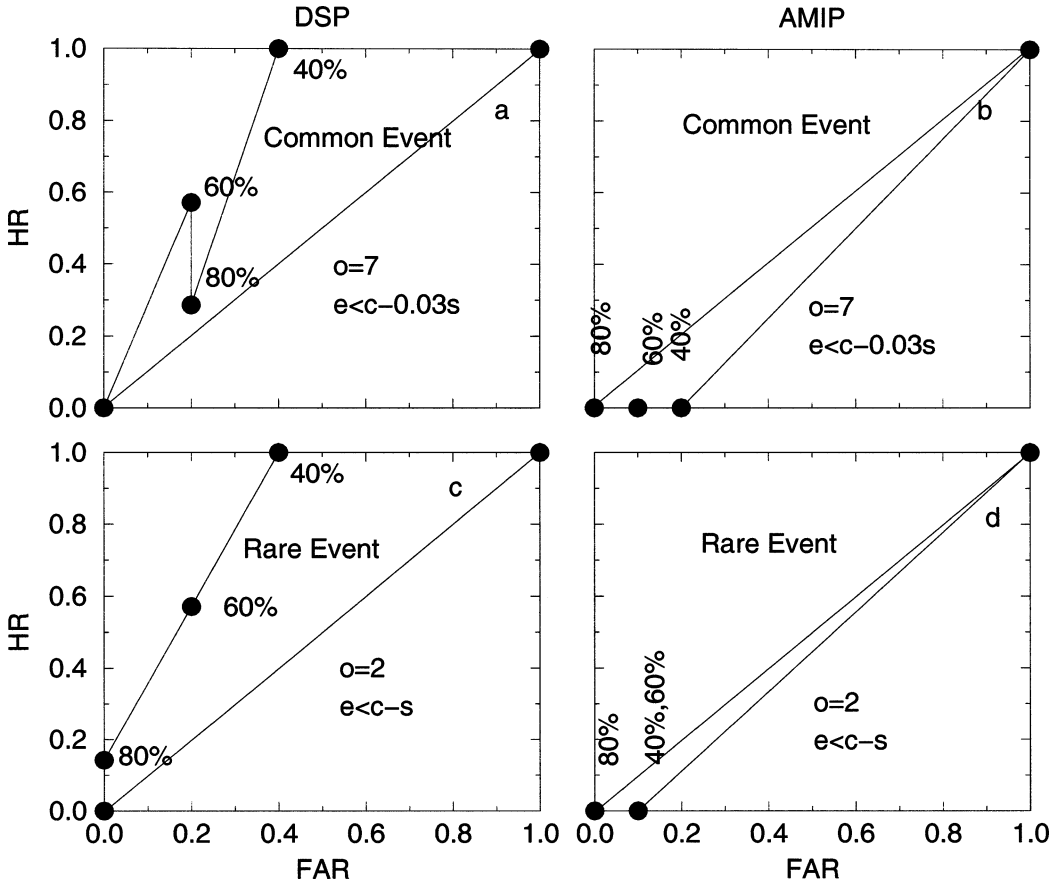

FIG. 13. Same as Fig. 11 but over SACZ.

- The distribution of the ensemble mean JFM precipitation rate over ARB and NOR from DSP-type runs conforms more closely to observations than the AMIP-type runs. However, the distribution of the precipitation rate over the subtropical regions of SACZ and ST are poor relative to observations in both DSP- and AMIP-type runs.
- The teleconnection of the ensemble mean JFM precipitation over a broad tropical area of South America (BTA in Fig. 1) with contemporaneous observed global SST is significant over the equatorial central and eastern Pacific Ocean in observations and in DSP-type runs. The AMIP-type runs show significant correlations of the ensemble mean JFM precipitation over BTA with subtropical oceans in both hemispheres, and in addition, show teleconnections with the tropical South Atlantic and central equatorial Pacific Oceans. The latter teleconnection is also seen, albeit weaker, in the DSP-type runs. The observational study of Paegle and Mo (2002) supports the teleconnections with the tropical Pacific and Atlantic Oceans.
- The skill of the DSP- and AMIP-type runs in predicting the interannual variability of mean JFM precipitation outperforms persistence in all four regions examined in this study. However, the DSP-type runs have a superior potential skill than the AMIP-type runs. It should be noted that the subtropical regions of SACZ and ST exhibited less skill than that over the tropical areas of NOR and ARB in both model-type runs.

We also examined the probabilistic skill and found that the DSP-type runs consistently had a superior skill to the AMIP-type runs in both common and rare occurrence events at all probability thresholds in all four regions examined in this study. In fact, the AMIP-type runs showed no skill at high probability thresholds over all four regions examined in this study except over NOR.

The poor skill in the AMIP-type model runs over South America is a result of the model drift while in the NOR region it has a higher skill as a result of the stronger SST–rainfall relationship. The persistently lower skill in the higher-latitude region of ST and SACZ in both DSP- and AMIP-type runs relative to the tropical regions of ARB and NOR suggests a certain lack of skill in tropical–extratropical interactions. It should also be pointed out that the SACZ region shows relatively

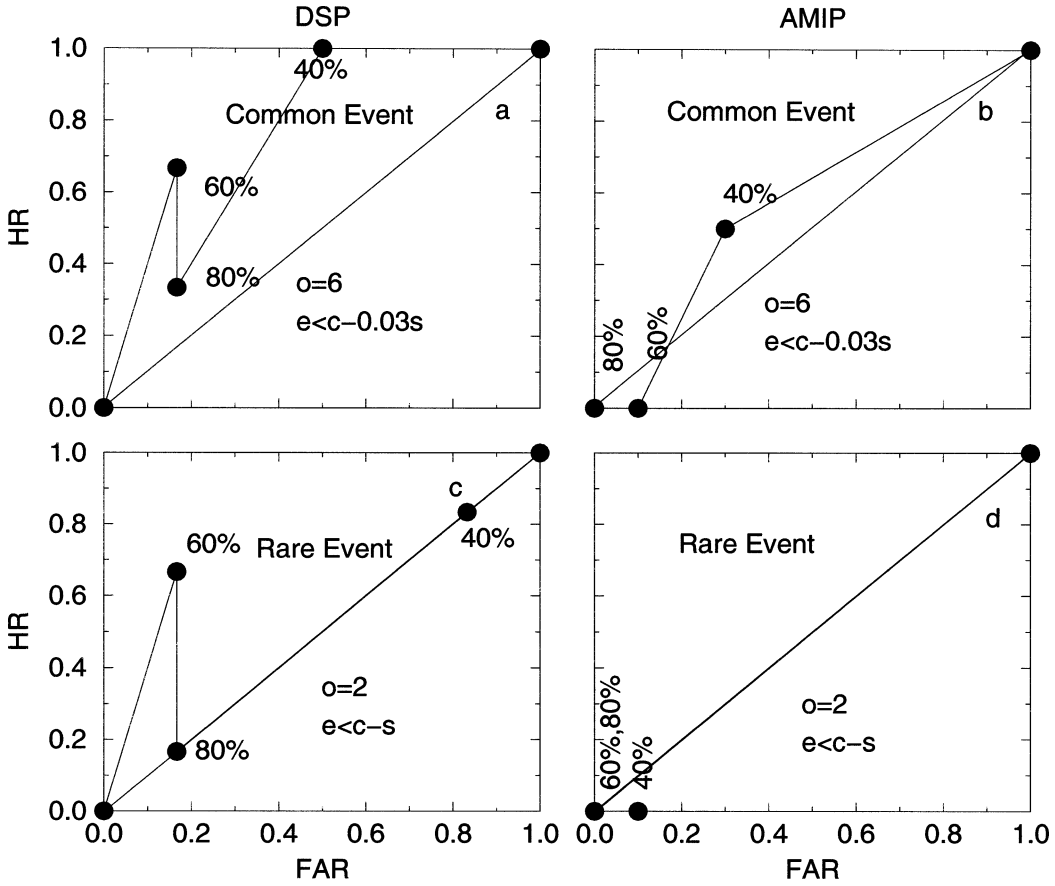

FIG. 14. Same as Fig. 11 but over ST.

higher skill than the ST region especially in the DSP-type runs (see Figs. 3, 10, 13c, and 14c) indicating that the observed SST plays a critical role in the model simulation over the region.

Acknowledgments. The author acknowledges the useful comments made by David Straus and an anonymous reviewer on an earlier version of the manuscript. This study was supported by NSF Grant ATM9814295, NASA Grant NAG5-11656, and NOAA Grant NA16GP2248.

APPENDIX A

Standard Deviation of the Distribution

The SD of the distribution is

$$\mathrm{SD}_i = \sqrt{\frac{1}{(n-1)}\sum_{j=1}^{n}(d_{ij}-\overline{d_i})^2}, \qquad \text{(A1)}$$

where, i refers to the bin, d_i is the ensemble mean of the number of years that the seasonal mean JFM precipitation falls into the bin i, and j refers to the ensemble members ($1 \cdots n$).

APPENDIX B

Normalized Standard Deviation

NSD is computed as

$$\mathrm{NSD} = \frac{\mathrm{SD}}{\mathrm{TSD}}, \qquad \text{(B1)}$$

where, standard deviation (SD) is

$$\mathrm{SD} = \frac{1}{N}\sum_{i=1}^{N}\sqrt{\frac{1}{(n-1)}\sum_{j=1}^{n}(x_{ij}-\overline{x_i})^2}, \qquad \text{(B2)}$$

where, x_{ij} is the climate variable for N years ($i = 1, \ldots N$) and n ensemble members ($j = 1, \ldots n$). Here $\overline{x_i}$ is the ensemble mean.

And, total standard deviation (TSD) is

$$\mathrm{TSD} = \sqrt{\frac{1}{N(n-1)}\sum_{i=1}^{N}\sum_{j=1}^{n}(x_{ij}-\overline{\overline{x}})^2}, \qquad \text{(B3)}$$

where $\overline{\overline{x}}$ is the climatological (ensemble) mean defined as

$$\overline{\overline{x}} = \frac{1}{Nn}\sum_{i=1}^{N}\sum_{j=1}^{n}(x_{ij}). \qquad \text{(B4)}$$

TABLE C1. Contingency table for ROC curves.

	Does ensemble probability for the event exceed threshold X?	
	Yes	No
Is the event observed?		
Yes	Hit (H)	Miss (M)
No	False alarm (FA)	Correct rejection (CR)

APPENDIX C

Relative operating characteristics

ROC curves are obtained by plotting hit rates (HR) against false alarm rates (FAR). The HR and FAR are essentially proportional to the observed frequency of the event and nonevent. Mathematically they may be expressed as

$$\mathrm{HR} = \frac{H}{H + M} \tag{C1}$$

$$\mathrm{FAR} = \frac{\mathrm{FA}}{\mathrm{FA} + \mathrm{CR}}, \tag{C2}$$

where, the variables on the rhs of the equations are defined in Table C1.

The greater the skill of the ensemble for a particular threshold, the more the ROC curve would bow toward the top left corner. Any point lying on or below the diagonal signifies no skill. The diagonal represents points for which HR equals FAR, which signifies climatology or a random forecast (Graham et al. 2000).

REFERENCES

Brankovic, C., and T. N. Palmer, 1997: Atmospheric seasonal predictability and estimates of ensemble size. *Mon. Wea. Rev.*, **125,** 859–874.

Campetella, C. M., and S. Vera, 2002: The influence of the Andes mountains on the South American low-level flow. *Geophys. Res. Lett.*, **29,** 1826, doi:10.1029/2002GL015451.

Cavalcanti, I. F. A., C. K. Folland, and A. W. Colman, 2002: Note on predictability of northeast Brazil rainfall and real-time forecast skill, 1987–98. *J. Climate*, **15,** 1993–1996.

Davies, R., 1982: Documentation of the solar radiation parameterization in the GLAS climate model. NASA Tech. Memo. 83961, 57 pp.

DeWitt, D. G., and E. K. Schneider, 1997: The Earth radiation budget as simulated by the COLA GCM. COLA Rep. 35, 39 pp. [Available from COLA, 4041 Powder Mill Rd., Suite 302, Calverton, MD 20705.]

Diaz, A. F., C. D. Studzinski, and C. R. Mechoso, 1998: Relationships between precipitation anomalies in Uruguay and southern Brazil and sea surface temperature in the Pacific and Atlantic Oceans. *J. Climate*, **11,** 251–271.

Dirmeyer, P. A. and F. J. Zeng, 1999: Precipitation infiltration in the Simplified SiB land surface scheme. *J. Meteor. Soc. Japan*, **78,** 291–303.

Fennessy, M. J., and Coauthors, 1994: The simulated Indian monsoon: A GCM sensitivity study. *J. Climate*, **7,** 33–43.

Folland, C. K., A. W. Colman, D. P. Rowell, and M. K. Davey, 2001: Predictability of northeast Brazil rainfall and real-time forecast skill, 1987–98. *J. Climate*, **14,** 1937–1958.

Fu, R., B. Zhu, and R. E. Dickinson, 1999: How do atmosphere and land surface influence seasonal changes of convection in the tropical Amazon? *J. Climate*, **12,** 1306–1321.

Gan, M., and V. B. Rao, 1994: The influence of the Andes cordillera on transient disturbances. *Mon. Wea. Rev.*, **122,** 1141–1157.

Gates, W. L., and Coauthors, 1999: An overview of the results of the Atmospheric Model Intercomparison Project (AMIP I). *Bull. Amer. Meteor. Soc.*, **80,** 29–55.

Graham, R. J., A. D. L. Evans, K. R. Mylne, M. S. J. Harrison, and K. B. Robertson, 2000: An assessment of seasonal predictability using atmospheric general circulation models. *Quart. J. Roy. Meteor. Soc.*, **126,** 2211–2240.

Harshvardhan, R. Davies, D. A. Randall, and T. G. Corsetti, 1987: A fast radiation parameterization for atmospheric circulation models. *J. Geophys. Res.*, **92** (D1), 1009–1016.

Kiehl, J. T., J. J. Hack, G. Bonan, B. A. Boville, D. L. Williamson, and P. J. Rasch, 1998: The National Center for Atmospheric Research Community Climate Model: CCM3. *J. Climate*, **11,** 1131–1149.

Kirtman, B. P., 2002: The COLA anomaly coupled model: Ensemble ENSO prediction. COLA Tech. Rep. 126, 32 pp. [Available from Center for Ocean–Land–Atmosphere Studies, 4041 Powder Mill Road, Suite 302 Calverton, MD 20705.]

——, D. A. Paolino, J. L. Kinter, and D. M. Straus, 2001: Impact of tropical subseasonal SST variability on seasonal mean climate simulations. *Mon. Wea. Rev.*, **129,** 853–868.

Krishnamurthy, V., and J. Shukla, 2001: Observed and model simulated interannual variability of the Indian monsoon. *Mausam*, **52,** 133–150.

Liebmann, B., G. N. Kiladis, J. A. Marengo, T. Ambrizzi, and J. D. Glick, 1999: Submonthly convective variability over South America and the South Atlantic convergence zone. *J. Climate*, **12,** 1877–1891.

Marengo, J. A., 1992: Interannual variability of surface climate in the Amazon Basin. *Int. J. Climatol.*, **12,** 853–863.

Mellor, G. L., and T. Yamada, 1982: Development of a turbulence closure model for geophysical fluid processes. *Rev. Geophys. Space Phys.*, **20,** 851–875.

Misra, V., P. A. Dirmeyer, and B. P. Kirtman, 2002: Regional simulation of interannual variability over South America. *J. Geophys. Res.*, **107,** 8036, doi:10.1029/2001JD900216.

——, ——, and ——, 2003: Dynamic downscaling of regional climate over South America. *J. Climate*, **16,** 103–117.

Moorthi, S., and M. J. Suarez, 1992: Relaxed Arakawa–Schubert: A parameterization of moist convection for general circulation models. *Mon. Wea. Rev.*, **120,** 978–1002.

Nobre, P., and J. Shukla, 1996: Variations of sea surface temperature, wind stress, and rainfall over the tropical Atlantic and South America. *J. Climate*, **9,** 2464–2479.

Paegle, J. N., and K. C. Mo, 1997: Alternating wet and dry conditions over South America during summer. *Mon. Wea. Rev.*, **125,** 279–291.

——, and ——, 2002: Linkages between summer rainfall variability over South America and sea surface temperature anomalies. *J. Climate*, **15,** 1389–1407.

Palmer, T. N., C. Brankovic, and D. S. Richardson, 2000: A probability and decision model analysis of PROVOST seasonal multimodel ensemble integrations. *Quart. J. Roy. Meteor. Soc.*, **126,** 2013–2034.

Parker, D. E., N. A. Rayner, E. B. Horton, and C. K. Folland, 1999: Development of the Hadley Centre sea ice and sea surface tem-

perature data sets (HADISST). *WMO Workshop on Advances in Marine Climatology-CLIMAR99*, Vancouver, British Columbia, Canada, Environment Canada, 194–203. [Available from Environment Canada, 4905 Dufferin St., Downsview, ON M3H 5T4, Canada.]

Robertson, A. W., and C. R. Mechoso, 1998: Interannual and decadal cycles in river flows of southeastern South America. *J. Climate,* **11,** 2570–2581.

Ropelewski, C. F., and M. S. Halpert, 1987: Global and regional scale precipitation patterns associated with the El Niño–Southern Oscillation. *Mon. Wea. Rev.,* **115,** 1606–1626.

——, and ——, 1989: Precipitation patterns associated with the high index phase of the Southern Oscillation. *J. Climate,* **2,** 268–284.

Shukla, J., 1998: Predictability in the midst of chaos: A scientific basis for climate forecasting. *Science,* **282,** 728–731.

——, and Coauthors, 2000: Dynamical seasonal prediction. *Bull. Amer. Meteor. Soc.,* **81,** 2593–2606.

Tiedtke, M., 1984: The effect of penetrative cumulus convection on the large-scale flow in a general circulation model. *Beitr. Phys. Atmos.,* **57,** 216–239.

Uvo, C., A. A. Repelli, S. E. Zebiak, and Y. Kushnir, 1998: The relationships between tropical Pacific and Atlantic SST and northeast Brazil monthly precipitation. *J. Climate,* **11,** 551–562.

Van den Dool, H. M., and Z. Toth, 1991: Why do forecasts for ''near normal'' often fail? *Wea. Forecasting,* **6,** 76–85.

Venegas, S. A., L. A. Mysak, and D. N. Straub, 1997: Atmosphere–ocean coupled variability in the South Atlantic. *J. Climate,* **10,** 2904–2920.

Wainer, I., and S. A. Venegas, 2002: South Atlantic multidecadal variability in the climate system model. *J. Climate,* **15,** 1408–1420.

Xie, P., and P. Arkin, 1996: Analysis of global monthly precipitation using gauge observations, satellite estimates and numerical model predictions. *J. Climate,* **9,** 840–858.

Xue, Y.-K., P. J. Sellers, J. L. Kinter, and J. Shukla, 1991: A simplified biosphere model for global climate studies. *J. Climate,* **4,** 345–364.

——, F. J. Zeng, and C. A. Schlosser, 1996: SSiB and its sensitivity to soil properties: A case study using HAPEX–Mobilhy data. *Global Planet. Change,* **13,** 183–194.

Zhou, J., and K.-M. Lau, 1998: Does a monsoon climate exist over South America? *J. Climate,* **11,** 1020–1040.